

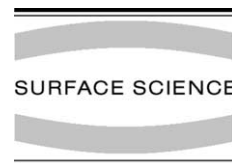


ELSEVIER

Available online at [www.sciencedirect.com](http://www.sciencedirect.com)

SCIENCE @ DIRECT®

Surface Science 537 (2003) 161–167



[www.elsevier.com/locate/susc](http://www.elsevier.com/locate/susc)

# The probing depth of total electron yield in the sub-keV range: TEY-XAS and X-PEEM

Bradley H. Frazer<sup>a,b,\*</sup>, Benjamin Gilbert<sup>c</sup>, Brandon R. Sonderegger<sup>a</sup>,  
Gelsomina De Stasio<sup>a</sup>

<sup>a</sup> Department of Physics, University of Wisconsin at Madison, Madison, WI 53706, USA

<sup>b</sup> Institute de Physique Appliquée, Ecole Polytechnique Fédérale de Lausanne, CH-1015 Lausanne, Switzerland

<sup>c</sup> Department of Earth and Planetary Sciences, University of California-Berkeley, Berkeley, CA 94720, USA

Received 4 April 2003; accepted for publication 24 April 2003

## Abstract

X-ray absorption spectra can be collected in multiple ways, each exhibiting a different probing depth. The total electron yield signal contains contributions from primary, Auger and secondary electrons. We present data on the total electron yield probing depth at core level energies ranging from 77 to 929 eV. By coating materials with chromium overlayers, we find that the maximum probing depth increases with core level energy from 15 to 141 Å. We demonstrate that the Auger electron contribution to total electron yield intensity is negligible, therefore X-ray absorption spectra acquired in X-ray PhotoElectron Emission spectroMicroscopy (X-PEEM) are equivalent to spectra acquired by total electron yield. We find that the signal intensity decreases exponentially with coating thickness, and that total electron yield probing depth and Auger electron range (calculated in the continuously slowing down approximation) are similar at low energies, but diverge for kinetic energies above 400 eV.

© 2003 Elsevier Science B.V. All rights reserved.

*Keywords:* X-ray photoelectron spectroscopy; X-ray absorption spectroscopy; Chromium

## 1. Introduction

In an X-ray absorption event, a primary core level electron is ejected leaving the system in an excited state (i.e. with a core hole). The system can relax via filling of the core hole by an electron of lower binding energy. This results in either the

emission of a fluorescence photon or in radiationless emission of an Auger electron. Inelastic electron electron scattering of the Auger electron results in a low energy secondary electron cascade [1,2].

The creation and detection of secondary electrons is fundamental for many techniques in surface science, including scanning electron microscopy, XANES and EXAFS spectroscopy, and for devices such as cathode ray tubes and microchannel plates [3–5]. In the case of XANES and EXAFS experiments, it is important to know the surface sensitivity of a particular probe, and its ability

\* Corresponding author. Address: Department of Physics, Synchrotron Radiation Center, University of Wisconsin at Madison, 3731 Schneider Dr., Stoughton, WI 53589, USA. Tel.: +1-6088772366; fax: +1-6088772001.

E-mail address: [bhfrazer@wisc.edu](mailto:bhfrazer@wisc.edu) (B.H. Frazer).

to collect or avoid signal from buried layers. The various techniques of monitoring fluorescence yield, partial electron yield and total electron yield (TEY) exhibit different surface sensitivities. Fluorescence yield has a large probing depth advantage over electron yield [6–8], but is often unsuitable for concentrated samples due to self absorption effects. In addition, core levels below 2 keV have higher a Auger electron yield than fluorescence yield per absorption event [9]. Auger electrons may be monitored directly in partial electron yield by selecting electrons of a particular kinetic energy. TEY has additional signal amplification following the cascade of electrons generated by the inelastic scattering of Auger electrons. No device to select electrons of a particular energy is needed, therefore the experimental set up is greatly simplified. The photocurrent is easily measured and represents the XANES or EXAFS signal [10,11].

This, however, leads to an uncertainty in the source of the signal. Without energy discrimination, primary, Auger and secondary electrons all contribute to the total yield photocurrent. All three types of electrons have different kinetic energies and mean free paths. In the near edge region, primary electrons have low kinetic energy and are incapable of creating large numbers of secondary electrons through inelastic scattering. The secondary electrons therefore are due almost entirely to inelastic scattering of the Auger electrons. It is generally accepted that TEY signal is dominated by the large number of low energy secondary electrons, therefore the TEY probing depth must largely depend on the range over which the Auger electrons inelastically scatter.

The mean free path of the low energy secondary electrons also affects the probing depth. Erbil et al. [12] have shown that for hard X-ray photons, the TEY is dominated by secondary electrons and have derived an expression for TEY signal versus sample depth. Several other experiments measured TEY from various materials at varying photon energies [12–19]. In the present paper, we report a systematic study of the TEY probing depth for a single over layer element (Cr), using six different substrates (Al, Si, Be, Ti, Fe and Cu) as Auger electron sources. We show that the TEY probing depth depends on the photon energy and therefore

on the Auger electron kinetic energy. We also compare the experimental results with Auger electron ranges calculated using the continuously slowing down approximation.

## 2. Experimental details

All X-ray absorption spectra (XAS) were acquired in the Spectromicroscope for the PHotoelectron Imaging of Nanostructures with X-rays (SPHINX), which is an X-ray PhotoElectron Emission spectroMicroscope (X-PEEM), installed at the University of Wisconsin Synchrotron Radiation Center (SRC) [20]. In this instrument the sample is held at high negative potential (–20 kV) and the photoelectrons are accelerated through and magnified by electron optics, composed of six magnetic lenses, a 30  $\mu\text{m}$  aperture and several stigmators and deflectors. The magnified photoelectron image is intensified by two microchannel plates and converted into a visible image by a phosphor screen. The final image is collected by a 12-bit digital camera and transferred to a computer. The SPHINX electron optics are tuned to a maximum transmission factor of 1 for electrons with 0.8 eV kinetic energy. Electrons with 100 and 1000 eV kinetic energy have transmission factors of  $9.2 \times 10^{-3}$  and  $9.9 \times 10^{-4}$ , respectively [21]. This device, therefore, strongly selects the secondary electron yield.

We acquired an image (180  $\mu\text{m}$  diameter) near a reference scratch on each sample, and collected the integrated spectral signal from the whole image while scanning the photon energy. After each subsequent coating step we returned to the same location on the sample surface, and acquired a new spectrum. Additionally, on several samples, TEY spectra were acquired by measuring the sample drain current immediately following the X-PEEM measurements.

The Al, Ti, Fe and Cu samples were polished with diamond paste down to 0.25  $\mu\text{m}$ , then UHV cleaned. The Si wafer and the 250  $\mu\text{m}$  thick Be foil did not require further polishing. All samples were sputtered with 1.5 keV argon ions for 20 min ( $1 \times 10^{-5}$  Torr) in the SPHINX UHV preparation chamber, prior to measurement.

Chromium was deposited via thermal sublimation at a typical pressure of  $2 \times 10^{-9}$  Torr (base pressure  $1 \times 10^{-10}$  Torr). The measurement chamber was typically at  $1 \times 10^{-10}$  Torr. Chromium deposition thickness was monitored using an Inficon<sup>®</sup> crystal thickness monitor. The beryllium and aluminum XAS spectra were acquired on the 062 6 m TGM beamline, while all other spectra were acquired on the 033 HERMON beamline at the SRC.

### 3. Results and discussion

Fig. 1a shows one series of X-ray absorption spectra acquired from the Fe sample before and after several Cr depositions. As Cr thickness increases, the spectral features of the Fe  $L_3$  and  $L_2$  edges (and all other edges described below) decrease in intensity while maintaining their line-shapes and energy positions. We therefore assumed that there were no chemical reactions with Cr, or oxidations, and used the most intense feature ( $L_3$  for Fig. 1) to measure the signal to background ratio of the under layer. All spectra acquired were normalized to the pre-edge region using a linear fit until, at high Cr coverage, the nonlinear beamline throughput curve ( $I_0$ ) began to dominate the background. At that point and thereafter, fifth order polynomial fits to the pre-edge region were used to normalize the spectra.

Fig. 1b shows corresponding Cr XAS spectra, for the same sample as Fig. 1a. When possible (the 6 m TGM does not reach the Cr 2p binding energy) Cr spectra were taken after each coating as a verification of the chromium deposition. To analyze the data from each sample, the substrate absorption peak to background ratio was computed for each value of Cr thickness. The peak ratios were normalized to the maximum value (from the data obtained without a chromium over layer) so the trend at all edges could be compared. These data are presented in Fig. 2a and b. Several features are evident from the figure. While less clear for the low energy Al, Si, and Be edges, the exponential nature of the decrease in peak intensity as a function of Cr thickness is evident for Ti, Fe and Cu edges. This decay is clear for all data in Fig. 2b, in which the natural logarithm of the peak

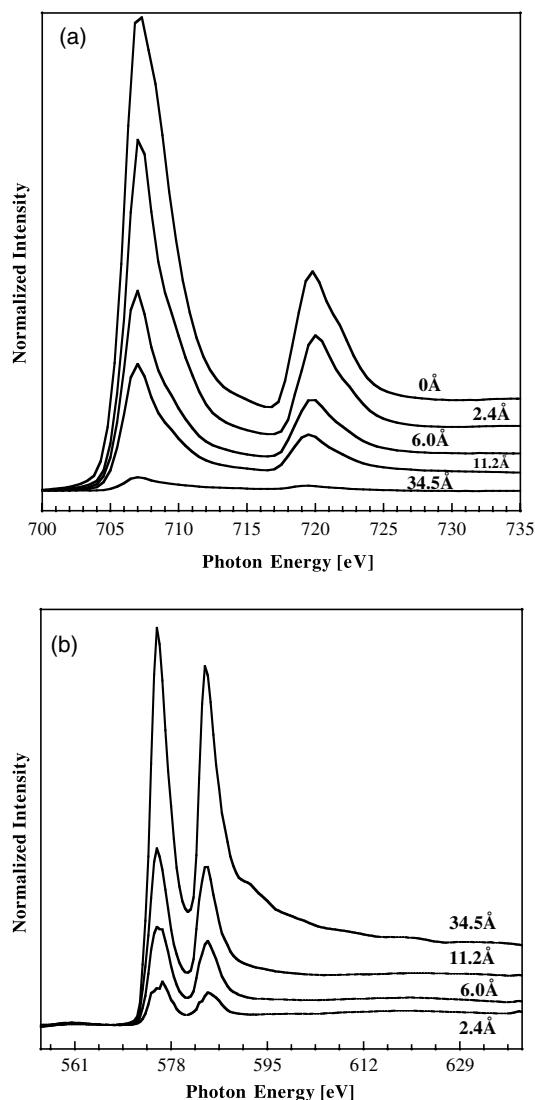


Fig. 1. (a) Fe 2p X-ray absorption spectra measured in SPHINX for 0, 2.4, 6.0, 11.2 and 34.5 Å Cr over layer thickness and (b) corresponding Cr 2p X-ray absorption spectra.

intensity are plotted as a function of Cr thickness. While Erbil et al. [12] predict and offer experimental evidence of a polynomial dependence of TEY signal as a function of over layer thickness in the hard X-ray range, reports exist in the literature for exponential dependence in the soft X-ray region [14,15,17,18].

We do note that for small values of Cr thickness (less than 5 Å) there seems to be a change of slope

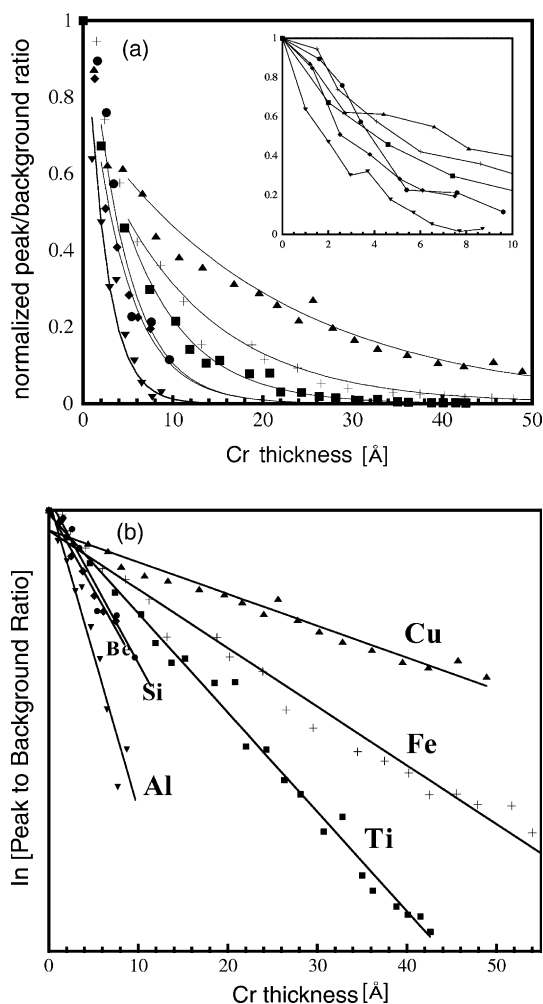


Fig. 2. (a) Peak to background ratio versus Cr thickness and (b) the natural logarithm of the peak to background ratio versus Cr thickness for various substrates. Markers represent experimental data, lines represent exponential and linear fits to the data. The exponential fits of (a) are calculated from the linear fits of (b). Fit values are given in Table 1. Lines of the exponential fits at low Cr thickness are not plotted in (a) since the fits and measured data diverge for small Cr thickness (inset of (a)). ( $\blacktriangle$  = Cu,  $+$  = Fe,  $\blacksquare$  = Ti,  $\blacklozenge$  = Be,  $\bullet$  = Si,  $\blacktriangledown$  = Al).

in Fig. 2a and b. The peak intensity drops much faster, with increasing coating thickness for Cr  $< 5$  Å compared to  $> 5$  Å. This might be explained by different contributions to the secondary electron yield, for example including the possibility of a short mean free path for secondary electrons, as suggested by some authors [15,22,23]. Another

possibility is surface topography at sub-monolayer Cr coverage as this is known to strongly affect the secondary electron yield in other systems [24]. The number of points in our data are too small to accurately fit this region to retrieve quantitative information on these speculations.

We performed linear fits and least square analysis of the data in Fig. 2b and found the gradient for each line, as reported in Table 1, with correlation coefficients between 0.97 and 0.99 for all data sets. The linear fit of each set of data enabled the extrapolation of data points corresponding to 0.1% peak to background ratio, which we define as the maximum probing depth. These extrapolated data, as well as characteristic Auger electron energy, and calculated Auger electron ranges are presented in Table 1.

We calculated the Auger electron range, that is, the range over which an Auger electron deposits its energy through inelastic scattering. Our calculation is based on the continuously slowing down approximation (CSDA) using energy dependent stopping powers from Ashley et al. [25]. Fig. 3a shows the electron stopping power  $S(E)$  in four different metals, calculated by Ashley et al. [25], as a function of electron kinetic energy. We are not aware of stopping powers for Cr in the literature, but considering that the values for the four metals of Fig. 3a do not differ considerably, we adopted the numerical average of the four as electron stopping power for Cr (also plotted in Fig. 3a).

Table 1

Peak photon energy  $h\nu$ , Auger electron kinetic energy  $E_{\text{Auger}}$ , Auger electron effective range (AER, calculated in the CSDA approximation as described in the text),  $1/e$  length of a linear fit to the natural logarithm of peak to background ratio versus Cr overlayer thickness, the correlation coefficient of the linear fit  $R$ , and the MPD extrapolated from the experimental data and linear fits of Fig. 2b for each edge

	$h\nu$ [eV]	$E_{\text{Auger}}$ [eV]	AER [Å]	$1/e$ length [Å]	$R$	MPD [Å]
Al L	77	68	19.5	2.1878	0.9707	15.5
Si L	101	76	20.1	4.1365	0.9742	29.3
Be K	120	104	21.8	4.2730	0.9892	29.5
Ti L	464	387	40.7	6.8339	0.9951	46.8
Fe L	707	651	60.7	11.559	0.9857	76.4
Cu L	929	920	84.1	21.322	0.9833	141

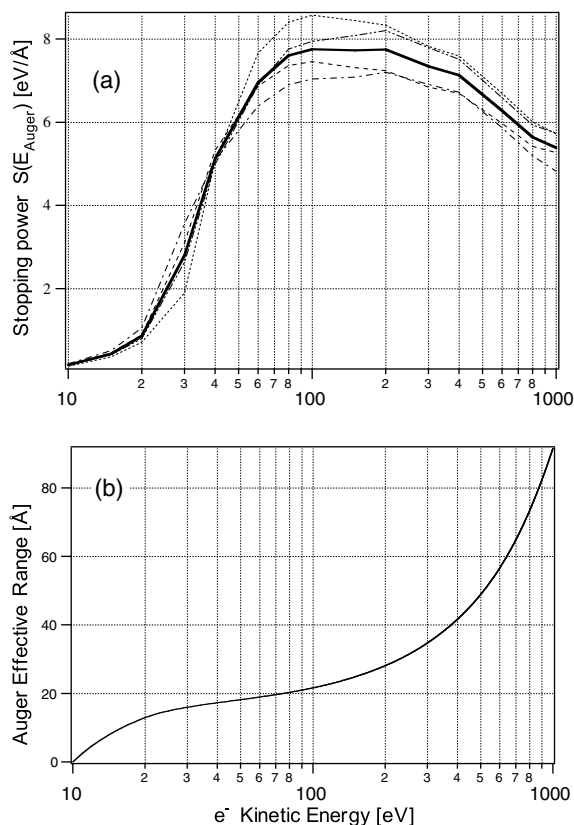


Fig. 3. (a) Stopping power  $S(E)$ , for Ni (···), Au (-·-·-), Cr (—), Cu (- - - -), and Ag (- - - - -) as a function of Auger electron kinetic energy. (b) AER as a function of electron kinetic energy calculated using Cr data from (a) in the CSDA.

The effective ranges for Auger electrons with different kinetic energies in Cr can then be calculated by numerically integrating:

$$R_{\text{CSDA}}(E_{\text{Auger}}) = \frac{1}{2} \int_{10 \text{ eV}}^{E_{\text{Auger}}} \frac{dE'}{S(E')} \quad (1)$$

where the 1/2 factor is derived from Monte Carlo simulations of electron ranges [12]. The result of this integration for each Auger electron kinetic energy of our experimental data is reported in Table 1, while the entire curve is shown in Fig. 3b.

The Auger effective range represents the distance over which one Auger electron of kinetic energy  $E_0$  interacts within the sample. While inelastically scattering, that electron generates additional electrons with kinetic energy  $< E_0$ , which in turn can undergo inelastic scattering with other

electrons. As this process propagates a large number of electrons are liberated within the sample, although only those cascading electrons that reach the surface with kinetic energy  $> 0$  can be detected.

Some authors [15,19] suggest that the TEY signal may consist of significant contributions from the primary Auger electrons as well as the high energy cascading electrons. They report several possible reasons for a smaller contribution of the secondary electrons to the TEY signal: the secondary electrons may have a smaller mean free path than the universal curve suggests, or they may experience reflection from the potential barrier at the surface of the sample [26]. Schroeder et al. have shown using conversion electron detection (CEY) that a significant portion of the TEY signal consists of electrons with at least 40 eV kinetic energy at the Ni K edge [19].

The effective energy filtering of the electron optics in SPHINX selects the low energy electrons but this bias is removed when collecting data by photocurrent TEY. Fig. 4 shows two series of Cu peak measurements. One curve represents data collected in SPHINX, the other photocurrent TEY. If the primary Auger electron contribution was relevant, the two curves should differ significantly. The curves of Fig. 4 are not identical but

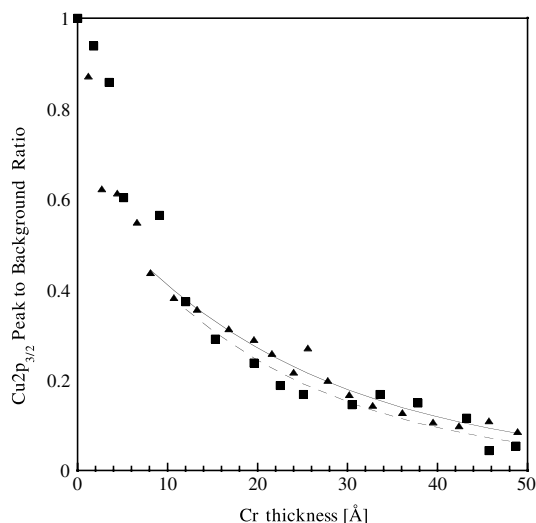


Fig. 4. Cu 2p peak to background ratio with exponential fits as acquired with SPHINX (data = ▲, fit = —) and TEY (data = ■, fit = - - -).

quite similar, and the probing depths are obviously comparable. We therefore conclude that at least in the case of chromium, the direct contributions of Auger electrons to the TEY signal are quite small. The only contribution of Auger electrons is therefore indirect, occurring through multiple inelastic scattering and X-PEEM XAS data may be considered equivalent to XAS measurements in TEY.

As reported in Table 1, our data show maximum probing depths (MPD) ranging from 15 to 141 Å, for Auger electrons of initial energies of 68–920 eV, respectively. In Table 1 we note the similarity between the measured maximum probing depth and the corresponding calculated Auger effective range below 400 eV. The data for MPD and Auger effective range (AER) are plotted in Fig. 5. The third order polynomial and exponential fits of Fig. 5 are merely shown as guides to the eye and are not meant to infer functional form. The two curves are similar in magnitude below 400 eV but show an increasing divergence as electron kinetic energy increases. This may be due to several effects. First, the values we used for the stopping power are not exact calculations for Cr and errors at low energies are propagated to higher energies as a consequence of the CSDA. Second, it has been shown that elastic scattering has a significant effect

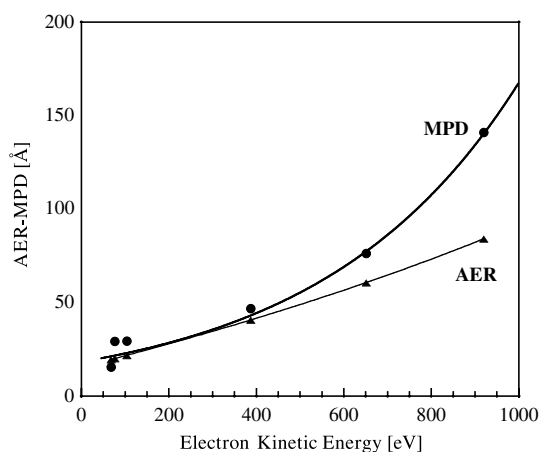


Fig. 5. Maximum probing depth (MPD, ●) and Auger effective range (AER, ▲) as a function of Auger electron initial kinetic energy. Lines are exponential and third order polynomial fits, respectively.

in increasing an electron's inelastic mean free path [27]. The third, and most probable cause of the observed discrepancy is that for soft X-ray core levels the MPD and the AER are not equivalent.

For hard X-ray core levels, the Auger effective range (200 to >1000 Å) is much larger than the secondary electron escape depth ( $\sim 5$  Å) [12,15]. As a consequence, there are many multiple inelastic scattering events resulting in a nearly uniform density of secondary electrons within 5 Å of the sample surface. In this case the TEY maximum probing depth is determined by the AER and the TEY signal versus sample depth can be expressed by a simple polynomial [12,19].

At lower energies the secondary electron escape depth is a sizable fraction of the AER (20–85 Å). The primary Auger electron undergoes a sizable portion of the total energy loss within 5 Å of the sample surface. The total number of multiple scattering events is smaller than at higher energies and the density of secondary electrons within 5 Å of the sample surface can no longer be considered uniform. In this case the AER is not the only factor in determining the MPD and the TEY signal versus sample depth is exponential [14,15,17,18]. For the very low energy core levels of Fig. 5, the total number of scattering events is quite small and thus the AER and MPD are in agreement.

For the Si 2p edge, we found a TEY maximum probing depth of 29.3 Å, which is considerably smaller than reported by Kasrai et al. [16]. The two measurements are not equivalent, however, as the over layer in their system is SiO<sub>2</sub>. Low energy electrons in a metal primarily scatter via interactions with valence band electrons. In insulating materials this does not occur, and consequently secondary electrons have larger escape depths. It is then expected that our maximum probing depth would be less than that measured with an insulating over layer, such as SiO<sub>2</sub>. In measuring the Ni 2p core level (853 eV) Abbate et al. [15] found a maximum probing depth of 25 Å (Tb over layer) while Vogel and Sacchi [18] find 60 Å (Dy over layer). Esteva et al. [14] report a  $1/e$  length of 7.2 and 11.3 Å for La and Gd L edges. These measurements are all consistent with our data considering that different materials are being investigated.

#### 4. Conclusions

We systematically measured the maximum probing depth for core level binding energies ranging from 77 to 929 eV. We found maximum probing depths for Cr metal ranging from 15.5 to 141 Å over this energy range. We also found that the decrease in peak intensity as a function of over layer thickness is exponential.

We used the energy filtering of the SPHINX X-PEEM to selectively collect secondary electrons, and compared the results with photocurrent TEY. We observed no significant differences, and prove that Auger electrons do not substantially contribute to the TEY signal. We therefore conclude that measuring only low energy electrons in X-PEEM is equivalent to measuring the TEY photocurrent.

We suggest that, for the core electron energies in the range 77–929 eV, the maximum probing depth is closely tied to the range over which an Auger electron deposits its energy. A comparison of the maximum probing depth data with approximate calculations of the effective Auger electron ranges suggests that the Auger range is on the order of the probing depth and, in fact, likely determines the depth sensitivity below 400 eV. The MPD is material dependent and also energy dependent. The divergence between the TEY MPD and AER with increasing core energy indicates a significant increase in the contribution from electron cascade, at least up to ~1 keV, which is not taken into account in the CSDA. To accurately predict the MPD in the soft X-ray region a detailed knowledge of the interactions of Auger electrons with the solid is essential. This theory should include corrections for elastic scattering of the Auger electrons as well as the number of cascading electrons generated by inelastic scattering, which rapidly increases with initial Auger electron kinetic energy in the soft X-ray range.

#### Acknowledgement

This work was performed at the University of Wisconsin Synchrotron Radiation Center which is

supported by NSF under Award No. DMR-0084402.

#### References

- [1] B.L. Henke, J.A. Smith, D.T. Atwood, *J. Appl. Phys.* 48 (1977) 1852.
- [2] B.L. Henke, J. Liesegang, S.D. Smith, *Phys. Rev. B* 19 (1979) 3004.
- [3] K.G. Hernqvist, *IEEE Trans. Constr. Electron.* 27 (1981) 117.
- [4] J.L. Wiza, *Nucl. Instrum. Methods* 162 (1991) 587.
- [5] W. Yi, S. Jin, T. Jeong, J. Lee, S.G. Yu, Y. Choi, J.M. Kim, *Appl. Phys. Lett.* 77 (2000) 1716.
- [6] L. Tröger, D. Arvantis, H. Rabus, L. Wenzel, K. Baberschke, *Phys. Rev. B* 41 (1990) 7297.
- [7] M. Kasrai, Z. Yin, G.M. Bancroft, K.H. Tan, *J. Vac. Sci. Technol. A* 11 (1993) 2694.
- [8] A. Hirayama, M. Watanabe, T.K. Sham, *Rev. Sci. Instrum.* 66 (1995) 1528.
- [9] M.O. Krause, *J. Phys. Chem. Ref. Data* 8 (1979) 307.
- [10] W. Gudat, C. Kunz, *Phys. Rev. Lett.* 29 (1972) 169.
- [11] T. Guo, M.L. denBoer, *Phys. Rev. B* 31 (1985) 6233.
- [12] A. Erbil, G.S. Cargill III, R. Frahm, R.F. Boehme, *Phys. Rev. B* 37 (1988) 2450.
- [13] R.G. Jones, D.P. Woodruff, *Surf. Sci.* 114 (1982) 38.
- [14] J.M. Esteve, R.C. Karnatak, J.P. Connerade, *J. Electron Spectrosc. Relat. Phenom.* 31 (1983) 1.
- [15] M. Abbate, J.B. Goedkoop, F.M.F. de Groot, M. Grioni, J.C. Fuggle, S. Hofmann, H. Pedersen, M. Sacchi, *Surf. Interface Anal.* 18 (1992) 65.
- [16] M. Kasarai, W.L. Lennard, R.W. Brunner, G.M. Bancroft, J.A. Bardwell, K.H. Tan, *Appl. Surf. Sci.* 99 (1996) 303.
- [17] T. Girardeau, J. Mimault, M. Jaouen, P. Chartier, G. Tourillon, *Phys. Rev. B* 46 (1992) 7144.
- [18] J. Vogel, M. Sacchi, *J. Electron Spectrosc. Relat. Phenom.* 67 (1994) 181.
- [19] S.L.M. Schroeder, G.D. Moggridge, R.M. Ormerod, T. Rayment, R.M. Lambert, *Surf. Sci.* 324 (1995) L371.
- [20] G. De Stasio, L. Perfetti, B. Gilbert, O. Fauchoux, M. Capozzi, P. Perfetti, G. Margaritondo, B.P. Tonner, *Rev. Sci. Instrum.* 70 (1999) 1740.
- [21] Ernst Bauer, personal communication.
- [22] T. Kaneko, *Surf. Sci.* 237 (1990) 327.
- [23] D.P. Pappas, K.P. Kämper, B.P. Miller, H. Hopster, D.E. Fowler, C.R. Brundle, A.C. Luntz, Z.X. Shen, *Phys. Rev. Lett.* 66 (1991) 504.
- [24] A. Hoffman, A. Laikhtman, S. Ustaze, M.H. Hamou, M.N. Hedhili, J.P. Guillotin, R. Azria, *J. Appl. Phys.* 91 (2002) 4726.
- [25] J.C. Ashley, J.C. Tung, R.H. Ritchie, V.E. Anderson, *IEEE Trans. Nucl. Sci.* NS-23 (1976) 1833.
- [26] A. Krol, C.J. Sher, Y.H. Kao, *Phys. Rev. B* 42 (1990) 3829.
- [27] A. Jablonski, *Surf. Interface Anal.* 21 (1994) 758.